From a bulk solid to thin films of a hybrid material derived from the [Ti10O12(cat)8(py)8] oxo-cluster and poly(4-vinylpyridine)

Bianca Patrahau, Clément Chaumont, Laurent Barloy, Petra Hellwig, Marc Henry, Frederic Melin, Pierre Mobian, Matthias Pauly

From a bulk solid to thin films of a hybrid material derived from the $[Ti_{10}O_{12}(cat)_8(py)_8]$ oxo-cluster and poly(4-vinylpyridine)

Bianca Patrahau,[a] Clément Chaumont,[a] Laurent Barloy,[a] Petra Hellwig,[b] Marc Henry,[a] Frédéric Melin,[b] Pierre Mobian,[* a] Matthias Pauly [c]

a) Laboratoire de Chimie Moléculaire de l'Etat Solide, UMR 7140 UDS-CNRS, Université de Strasbourg, 4 rue Blaise Pascal, F-67000 Strasbourg, France

b) Laboratoire de Bioélectrochimie et Spectroscopie, UMR 7140 UDS-CNRS, Université de Strasbourg, 4 rue Blaise Pascal, F-67000 Strasbourg, France

c) Polyélectrolytes, Complexes et Matériaux, Institut Charles Sadron, CNRS, Université de Strasbourg, 23 Rue du Loess,F- 67200 Strasbourg, Strasbourg, France

Corresponding author : mobian@unistra.fr

Abstract:

In this work, we report the formation of a coloured inorganic-organic hybrid material generated from the $[Ti_{10}O_{12}(cat)_8(py)_8]$ (catecholato (cat), pyridine (py)) oxo-cluster and poly(4-vinylpyridine). The titanium oxo-cluster is linked to the organic polymer through Ti-N coordination bonds. Vibrational spectroscopies (FT-IR and Raman scattering) and thermo gravimetric analysis highlight a quantitative incorporation of the cluster in the polymeric matrix with no degradation of the inorganic core of the starting complex and highlight the good homogeneity of the resulting materials. The solid-state NMR measurements (^{13}C CP-MAS) also reveal that the hybrid material results only from the substitution of the labile pyridine ligands within $[Ti_{10}O_{12}(cat)_8(py)_8]$ by the pyridines of the P4VP polymer. Next, the functionalization of SiO_2 surfaces with monolayer or multilayer films composed of alternate layers of the oxo-cluster and of the polymer is detailed. The thickness of these films, as evaluated by ellipsometry, ranges from a few nanometers to tens of nanometers for the monolayer films and the multilayer films respectively.

Introduction

Inorganic-organic hybrids[1] are fascinating materials owing to the synergetic influence of the organic and inorganic constituents on the overall properties of these materials. Hybrid materials have found applications in various fields such as photo-catalysis,[2] biology and medicine,[3] functional coatings,[4] micro-optics and micro-electronics.[5] Titanium oxo-clusters are particularity attractive nano-building blocks (NBBs) for the generation of hybrid materials, as their highly diverse structures[6] are usually perfectly established, as the degree of condensation O/Ti is controlled and as, in some cases, their integrity is preserved during the assembly with the organic counter-part. Sanchez *et al.* have reviewed the different bottom-up strategies permitting to synthesise inorganic-organic hybrid materials based on titanium oxo-clusters.[7] A first strategy involves the NBBs in the presence of templating agents such as surfactants, amphiphilic or double hydrophilic block copolymers leading to the formation of mesostructured hybrid arrangements.[8] A second strategy implies a copolymerization between an organic monomer and polymerizable groups decorating the inorganic core of the oxo-cluster.[9] In this case, these oxo-clusters are generally synthesized through a post-functionalisation step. Therefore, strong covalent bonds are created in such hybrid materials between the oxo-clusters and the organic polymer matrix.

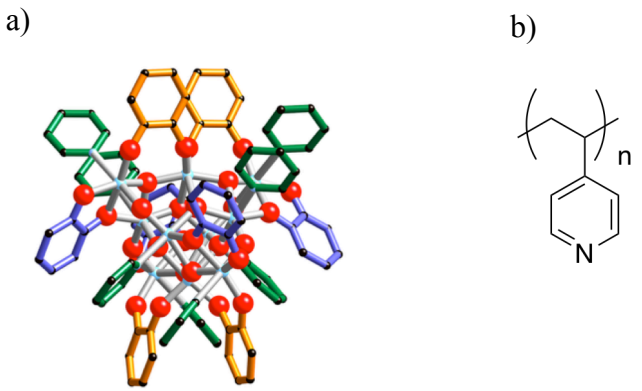

Figure 1: Molecular structure of (a) $[Ti_{10}O_{12}(cat)_8(py)_8]$ and (b) P4VP polymer. The sketch of the complex evidences the S_4-symmetry. The two inequivalent catecholato ligands are differently coloured (in orange and blue). The pyridine ligands are coloured in green, the titanium atoms in blue and the oxygen atoms are in red. The hydrogens are omitted for clarity.

In that context, we have reported a robust S_4-symmetry titanium-based architecture bearing catecholato (cat) and pyridine (py) ligands.[10] This neutral complex formulated as

$[Ti_{10}O_{12}(cat)_8(py)_8]$ displays a tetrahedral inorganic core decorated by catecholato ligands (the molecular crystal structure of the complex is shown in Figure 1a). In solution, the pyridine ligands are labile and can be exchanged by substituted pyridine ligands.[11] Furthermore, this complex exhibits the distinguishing feature of absorbing visible light, owing to charge transfer between the lone pair of oxygen atoms and the empty 3d orbitals of the Ti(IV) ions.[12]

Colour is indeed a major property to be considered when titanium(IV)-based hybrid materials have to be designed. This requirement arises from the possibility to generate photo-active hybrids acting in the visible domain, in opposition to TiO_2 that is mostly a UV-active material. Thus, great efforts are actually devoted to generate coloured titanium(IV) hybrids or coloured titanium oxo-cluster NBBs as hybrid precursors.[13]

Therefore, $[Ti_{10}O_{12}(cat)_8(py)_8]$ could be viewed as a promising nano-object precursor to access unprecedented hybrids by exploiting the labile behaviour of the nitrogen monodentate ligands. In this work, we report an unique way to form Ti(IV)-based inorganic-organic hybrid coloured materials and thin films based on the $[Ti_{10}O_{12}(cat)_8(py)_8]$ architecture. In these systems, the linkage of the titanium oxo-cluster and the organic polymer implies Ti-N coordination bonds.[14] The preparation and the full characterization of the bulk hybrid material and the related thin films derived from the $[Ti_{10}O_{12}(cat)_8(py)_8]$ oxo-cluster and poly(4-vinylpyridine) (P4VP) are described hereafter.

Results and discussion

Synthesis and thermal characterization

The incorporation of metallic complexes within a polymeric matrix is known to modify the initial properties of the polymer, such as the viscosity or the glass transition. Complexation of P4VP with transition metal complexes such as copper,[15] nickel,[16] cadmium[17] or ruthenium[18] complexes has already been reported. Thus, we plan to take advantage of the labile behaviour of the pyridine ligands in $[Ti_{10}O_{12}(cat)_8(py)_8]$ to coordinate the P4VP polymer to this oxo-cluster. A chloroform solution of $[Ti_{10}O_{12}(cat)_8(py)_8]$ is added dropwise to a chloroform solution of P4VP (average MW ~60,000 $g.mol^{-1}$) to generate hybrids named as P4VPTiXX% (where XX % represents the mass percentage calculated as the mass of $[Ti_{10}O_{12}(cat)_8(py)_8]$ divided by the total mass of the solid mixture (P4VP and $[Ti_{10}O_{12}(cat)_8(py)_8]$). Importantly, we distinguish initial complex $[Ti_{10}O_{12}(cat)_8(py)_8]$ with the oxo-cluster incorporated in the polymeric matrix. Thus, the oxo-cluster within the hybrid material is labelled as Ti10. Only for hybrids where XX % are superior or equal to 10%, we notice the formation of an orange

precipitate, which is isolated and dried under vacuum. For hybrids with lower mass percentage, the resulting solutions are concentrated under vacuum to afford the desired hybrids. Following this procedure, P4VPTiXX% where XX = 1, 2, 3, 4, 5, 10, 13, 15, 17, 20, 33 and 50 are obtained. The isolated solids are analysed by thermogravimetric analysis (TGA) and the thermograms obtained for $[Ti_{10}O_{12}(cat)_8(py)_8]$, P4VP, P4VPTi20%, P4VPTi33% and P4VPTi50% are shown in Figure 2a. These analyses are performed under air to determine the percentage of residual TiO_2 obtained at high temperature.

a)

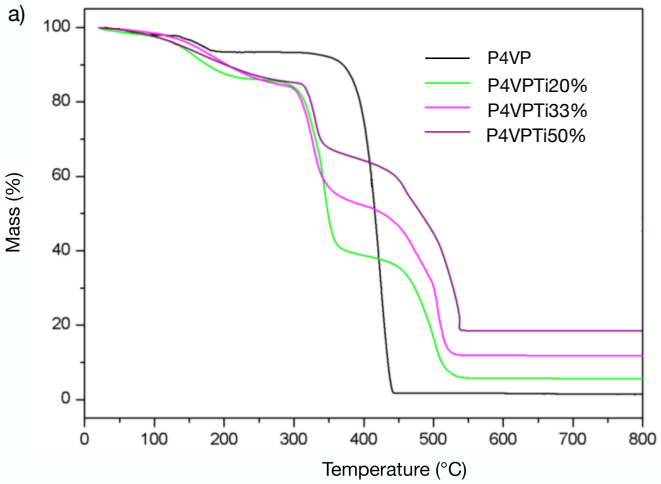

b)

Hybrid	TiO_2 mass % (calcd.)	TiO_2 mass % (exp.)
P4VPTi20%	7	6.7
P4VPTi33%	12	11.8
P4VPTi50%	19.4	18.3

Figure 2: a) Thermograms obtained under air at 10°C.min^{-1} for the analysis of P4VP, P4VPTi20%, P4VPTi33% and P4VPTi50%. b) Mass percentage of residual TiO_2 at 700°C (calculated and experimental).

Two weight losses are observed for the P4VP analysis. The first one (≈ 6%) is attributed to the dehydration of the polymer at around 150°C whereas the most important loss (94%) at 420°C is linked to the degradation of the polymer. The thermograms of the three analysed hybrids, that are dissimilar to those of P4VP and $[Ti_{10}O_{12}(cat)_8(py)_8]$ (see supporting information), show a very close similarity. Interestingly, a pronounced weight loss assigned to the total or partial degradation of the P4VP backbone within the hybrids is observed at 340°C. We assume that the decrease of the thermal stability ($\Delta T \approx 80$°C) of the organic polymeric chain within the hybrid material in comparison with the P4VP arises from the coordination of the oxo-cluster to the P4VP pyridine rings.[19] The Lewis acid character of titanium (IV) coordinated by the pyridines could explain this decrease of thermal stability. Next, a second pronounced weight loss occurs, originating from the degradation of the rest of the organic matter within these hybrids. An excellent match is found between calculated percentages of residual TiO_2 and those determined experimentally at 700°C for all the analysed hybrids (see

the table in Fig. 2b). Overall, this thermal analysis proves that the synthetic procedure applied to generate the hybrid materials is quantitative, since all the titanium within the oxo-cluster is efficiently incorporated in polymeric matrix. In order to gain deeper information about the interaction existing between the oxo-cluster and the P4VP component, these hybrids are then studied by vibrational spectroscopy.

Infrared and Raman spectroscopy

We focused our attention to the most relevant region of the FT-IR spectra of these materials, i. e. between 1570 and 1675 cm^{-1} that is assigned to the stretching of the pyridine C-N bonds (Figure 3a). As it was already observed for the coordination of transition metals to pyridine rings,[20] the C-N stretch band of P4VP is shifted towards higher energies ($\Delta\upsilon \approx 20$ cm^{-1}) upon coordination to the cluster. For P4VPTi50%, the C-N stretch band assigned to the coordinated pyridine C-N bonds is more intense in comparison with the one recorded for P4VPTi20%. Owing to its complexity, it is impossible to assign the Ti-N and Ti-O stretches in the region between 900 cm^{-1} and 400 cm^{-1} (see Figure 3b). However, a band at υ = 475 cm^{-1} clearly increases when the amount of the oxo-cluster incorporated in the polymer increases. This band may be assigned to the Ti-N stretch according previous studies.[21] Also, the infrared spectrum of P4VPTi20% is subtracted to the spectrum of P4VP to verify if the structural integrity of the oxo-cluster within the hybrid is identical to $[Ti_{10}O_{12}(cat)_8(py)_8]$. This subtracted spectrum resembles strongly the infrared signature of $[Ti_{10}O_{12}(cat)_8(py)_8]$; however it some differences appear also, in particular in the region around 1600 cm^{-1} (Figure 3b). This indicates that the main core of the oxo-cluster within the material remains identical to $[Ti_{10}O_{12}(cat)_8(py)_8]$, but also that chemical interactions occur between the polymer matrix and the cluster.

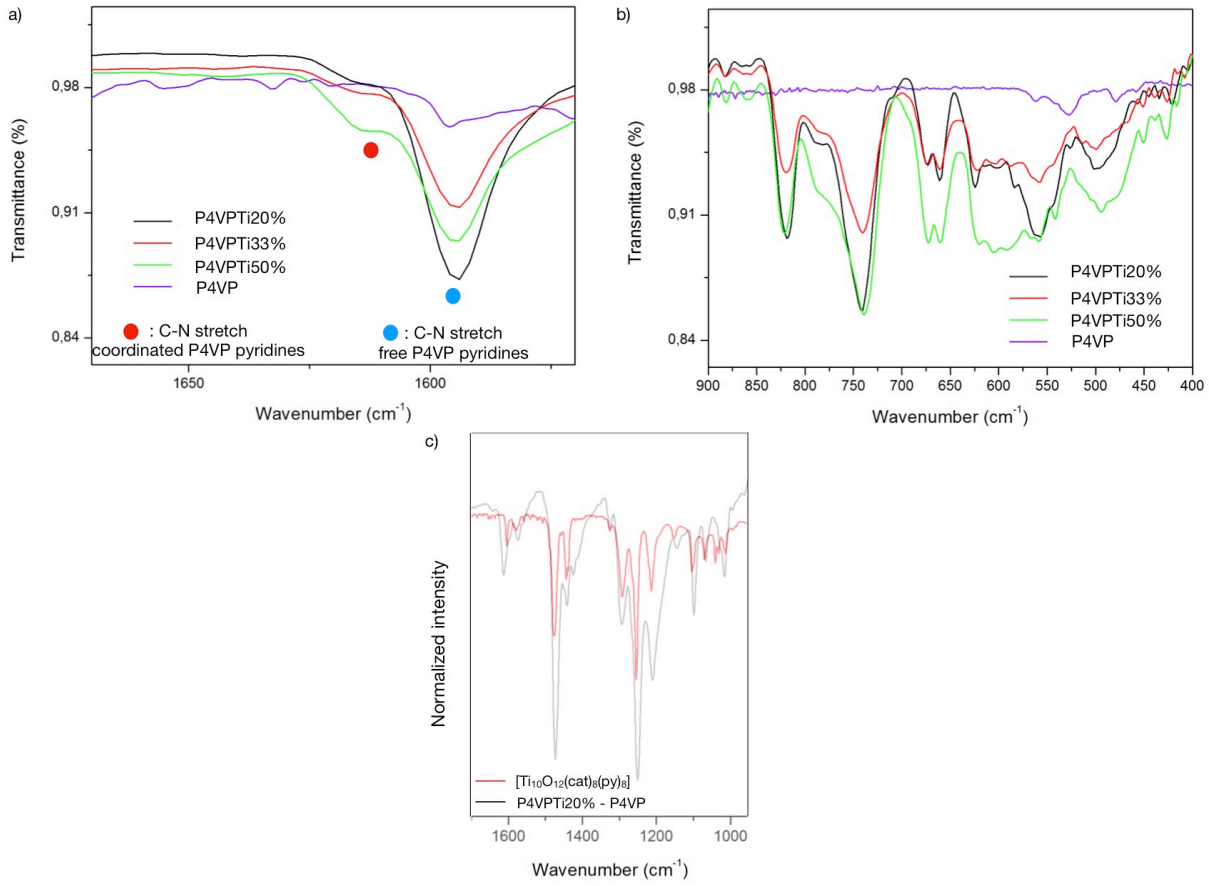

Figure 3: a) Infrared spectra of P4VP, P4VPTi20%, P4VPTi33% and P4VPTi50% (region between 1570 and 1675 cm^{-1}). The bands marked with the blue spot are attributed to the C-N stretch of the free pyridine rings, while those marked with the red spot are attributed to the C-N stretch of the coordinated pyridine rings. b) Infrared spectra of P4VP, P4VPTi20%, P4VPTi33% and P4VPTi50% (region between 900 and 400 cm^{-1}). c) Subtracted spectrum P4VPTi20% minus P4VP and superimposition with the infrared spectrum of $[Ti_{10}O_{12}(cat)_8(py)_8]$ (region between 1700 cm^{-1} and 950 cm^{-1}).

In addition to the infrared spectroscopy analysis, the Raman spectra are recorded for $[Ti_{10}O_{12}(cat)_8(py)_8]$ and for the hybrid materials P4VPTiXX% (XX = 1, 3, 5, 10, 15, 20). The assignments of several vibrational bands of the $[Ti_{10}O_{12}(cat)_8(py)_8]$ spectra were carried out (the spectrum is shown in the Supporting Information).

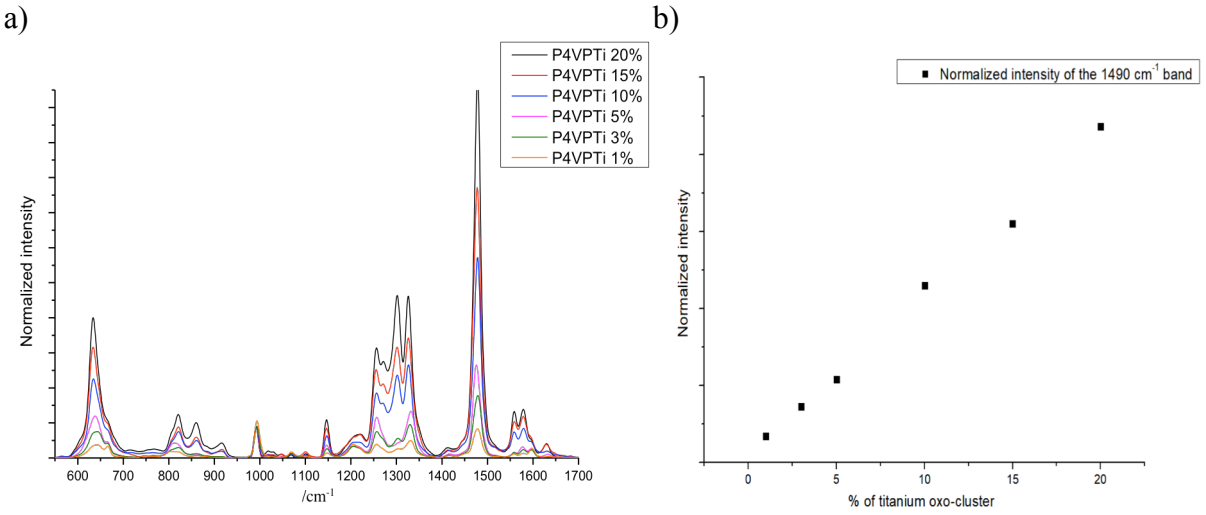

Figure 4: a) Superimposition of the P4VPTiXX% (XX = 1, 3, 5, 10, 15, 20) Raman spectra. b) Plot of the intensity of the band situated at 1490 cm^{-1} as a function of XX in P4VPTiXX% (XX = 1, 3, 5, 10, 15, 20). The baseline of all the spectra are corrected and brought to the same intensities by using the peak situated at 993 cm^{-1} which corresponds to the υ_8 vibration mode of P4VP.[22]

According to the literature, the band at 1295 cm^{-1} corresponds to the C-O elongation while the elongations of the C-C bonds are centred between 1495 cm^{-1} and 1580 cm^{-1}.[23] Importantly, the elongation of the Ti-O bonds is found at 633 cm^{-1}. This wavenumber is fully consistent with the Raman shift obtained for the Ti-O bonds in a related complex.[24] The normalized Raman spectra extracted from the analysis of the hybrid materials are displayed in Figure 4a. These spectra display vibration bands found either in the $[Ti_{10}O_{12}(cat)_8(py)_8]$ spectra or P4VP spectra and also new bands (see Supporting information). A linear increase of the intensity of several bands correlated to the amount of titanium incorporated within the analysed material is observed. The plot of the relative intensity of the most intense band at 1490 cm^{-1} versus XX (in P4VPTiXX%) (Figure 4b) proves their linear relationship. This confirms the conclusions drawn from the TGA studies, which indicate that the $[Ti_{10}O_{12}(cat)_8(py)_8]$ cluster is quantitatively incorporated in the organic P4VP matrix throughout the synthesis of the hybrid material.

Importantly, for all the hybrid materials tested, when the Raman measurement is performed at various points of a given sample, very similar spectra in terms of energy and intensity are recorded. This reflects the good homogeneity of these solids.

^{13}C CP-MAS Analysis

These solids were also studied through solid-state ^{13}C CP-MAS NMR. The spectra of P4VP, $[Ti_{10}O_{12}(cat)_8(py)_8]$ and P4VPTi20% are recorded and discussed in relation to the solid-state ^{13}C NMR signature of a powder mixture composed of $[Ti_{10}O_{12}(cat)_8(py)_8]$ and P4VP (20% w/w) (see Figure 5). The ^{13}C CP-MAS NMR spectrum of $[Ti_{10}O_{12}(cat)_8(py)_8]$ (Figure 5d) shows only signals in the aromatic region with three large signals and for the most deshielded carbons four sharp signals at δ = 159.07 ppm, 156.30 ppm, 155.74 ppm, 153.26 ppm. These signals are undoubtedly attributed to the C-O resonances within this S_4-symmetry complex. An identical observation for the complex in solution had been made.[10] Concerning the ^{13}C CP-MAS NMR signature of P4VP (Figure 5c), in addition to the two very large signals in the aromatic region attributed to the resonance of the pyridine carbons, a large signal around 40 ppm is observed belonging to the alkyl carbons of the polymer. Spectra which are very similar to the one obtained for P4VP (Figure 5c) are recorded for the hybrid material P4VPTi20% (Figure 5b), and for the powder mixture composed of $[Ti_{10}O_{12}(cat)_8(py)_8]$ and P4VP (20 % w/w) (Figure 5a).[25]

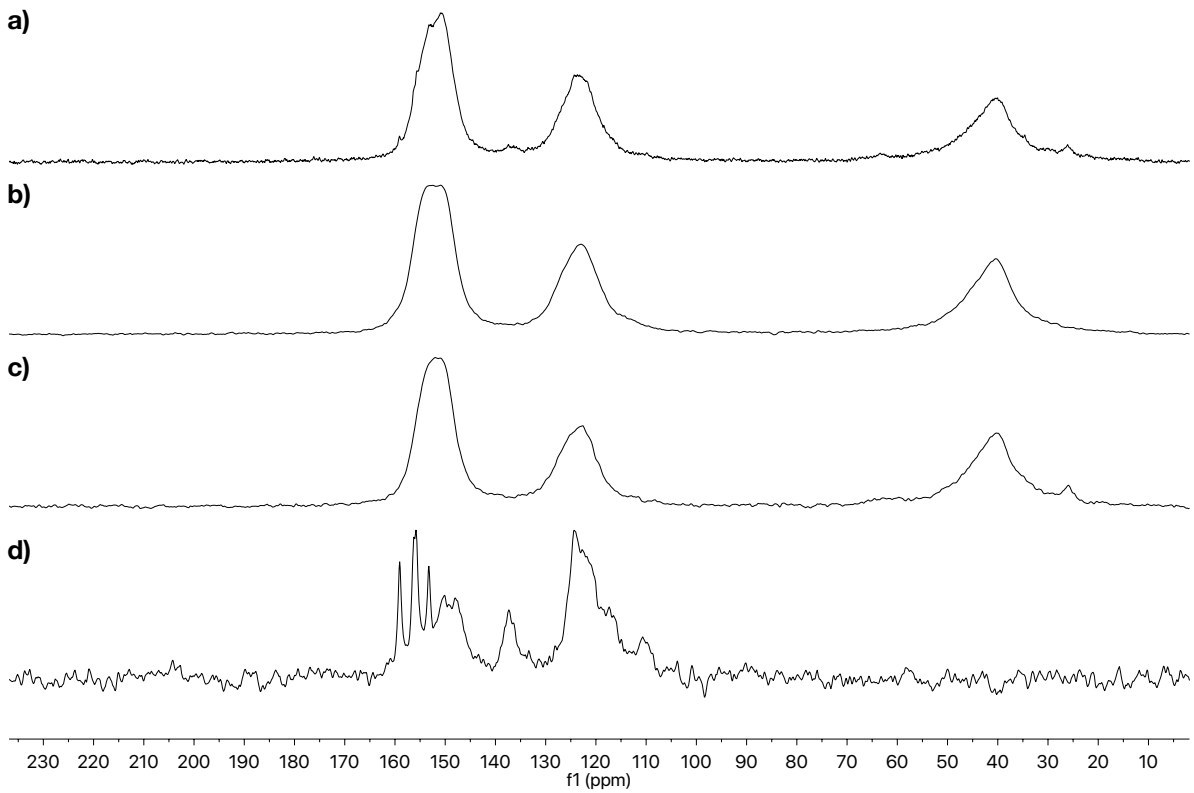

Figure 5: ^{13}C CP-MAS NMR spectrum of a) a powder mixture composed of $[Ti_{10}O_{12}(cat)_8(py)_8]$ and P4VP (20 % w/w); b) P4VPTi20%; c) P4VP and d) $[Ti_{10}O_{12}(cat)_8(py)_8]$.

Next, the P4VPTi20% spectrum is subtracted from the spectrum of P4VP (Figure 6a) and the powder mixture spectrum is subtracted from the spectrum of P4VP (Figure 6b). Both substracted spectra are clearly different. The trace displayed in Figure 6b appears almost identical to the spectrum of $[Ti_{10}O_{12}(cat)_8(py)_8]$ (Figure 6c), indicating that the spectrum of the mixture (Figure 5a) solely results from the superimposition of the spectra of its two constituents, *i.e.* those of $[Ti_{10}O_{12}(cat)_8(py)_8]$ and P4VP. Furthermore, it shows that the mixing of the two powders does not affect the $[Ti_{10}O_{12}(cat)_8(py)_8]$ molecular structure. In contrast, the second trace (Figure 6a) exhibits no similarity with the $[Ti_{10}O_{12}(cat)_8(py)_8]$ spectrum. This analysis proves that P4VPTi20% results from the assembly of the P4VP polymer with the cluster. Additionally, according to infrared analysis, there is no doubt that the $Ti_{10}O_{12}(cat)_8$ core with the hybrid material remains very close as the one established by X-ray analysis for $[Ti_{10}O_{12}(cat)_8(py)_8]$. Consequently, this indirectly proves again that the formation of the hybrid material results only from the substitution of the labile pyridine ligands within $[Ti_{10}O_{12}(cat)_8(py)_8]$ by the pyridine rings of the P4VP polymer.

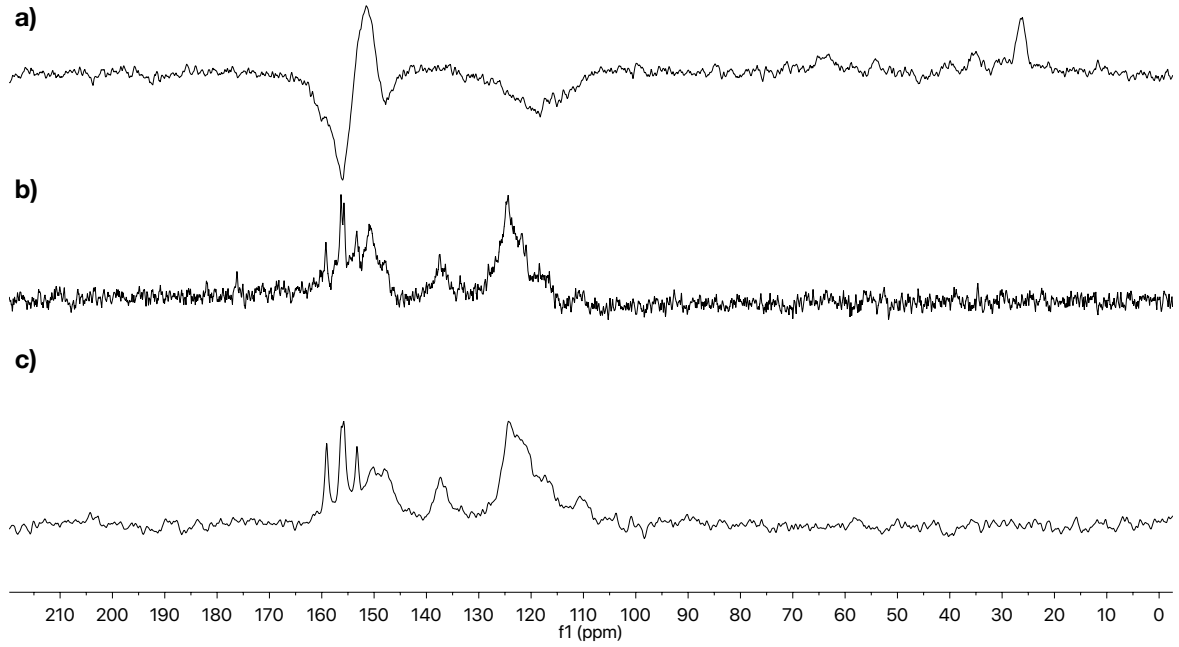

Figure 6: Subtracted ^{13}C CP-MAS NMR spectra: a) P4VP minus P4VPTi20%, b) the P4VP minus the powder mixture of $[Ti_{10}O_{12}(cat)_8(py)_8]$ and P4VP (20 % w/w). For comparison purposes, the NMR spectrum of $[Ti_{10}O_{12}(cat)_8(py)_8]$ is shown in c).

Light absorption properties

Titanium(IV)-based hybrid materials absorbing light in the visible domain is a really active domain driven by potential unprecedented photoredox properties of these materials.[13] As $[Ti_{10}O_{12}(cat)_8(py)_8]$ is highly absorbing in the visible domain (λ_{max} = 411 nm, ε = 10800 $L.mol^{-1}.cm^{-1}$),[10] we investigate the solid-state UV-Visible optical properties of P4VPTi20%, P4VPTi33% and P4VPTi50%. Figure 7 displays the Kubelka-Munk function[26] extracted from diffuse reflectance spectra recorded for these materials as well as for P4VP and $[Ti_{10}O_{12}(cat)_8(py)_8]$ alone. The hybrid materials absorb light in the visible domain below 650 nm whereas P4VP only absorbs in the UV domain. The spectra of the hybrid materials closely resemble the one recorded for $[Ti_{10}O_{12}(cat)_8(py)_8]$. The absorption edges are found to be 2.05 eV, 2.0 eV and 1.95 eV for P4VPTi20%, P4VPTi33% and P4VPTi50% respectively showing a shift as the loading amount of Ti(IV) increases. Since the colour of these materials is originated from charge transfer between the lone pairs of the catecholato oxygen atoms and the Ti(IV) ions, and since a long Ti-O bond absorbs light at lower energy compared to a short

Ti-O bond, this highlights shorter Ti-O bonds within the hybrid with low titanium loading and longer Ti-O bonds for P4VPTi50%. So, attractive interactions between the catecholato ligands and their environments within the hybrids with high Ti10 concentrations explain the Ti-O bonds elongation. In the case of P4VPTi20%, repulsive interactions occurred between the catecholato ligands and their environments inducing the Ti-O bonds shortening.

Concerning solid-state emission properties, P4VP is a good light emitter (425 nm) upon excitation at 330 nm. For the hybrids polymers, even for very low Ti loading (*e.g.* P4VPTi1%), several excitation wavelengths are tested but no emission is detected. Obviously, the oxo-cluster acts as a fluorescence quencher. This result linked to the emission properties of the hybrid is unsurprising since the same observation was made for monomeric titanium-based complexes.[27]

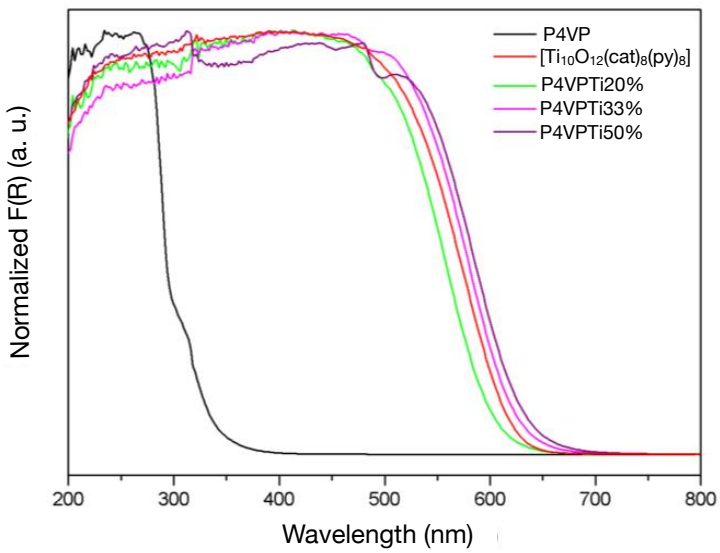

Figure 7: F(R) recorded for P4VPTi20%, P4VPTi33%, P4VPTi50%, P4VP and $[Ti_{10}O_{12}(cat)_8(py)_8]$. F(R) is the Kubelka-Munk function.[26]

Surfaces functionalized by hybrid thin films

The design of functional "smart" surfaces is a constant demand in modern material science. Also, it is well known that P4VP forms films on glass or quartz surfaces through hydrogen bonds, allowing the grafting on this surface of metal complexes or nanoparticles.[28] Therefore, we have examined the formation of hybrid films incorporating the cluster *via* the

functionalization of a surface by the P4VP. The schematic principle of the functionalization of a surface is displayed in Figure 8.

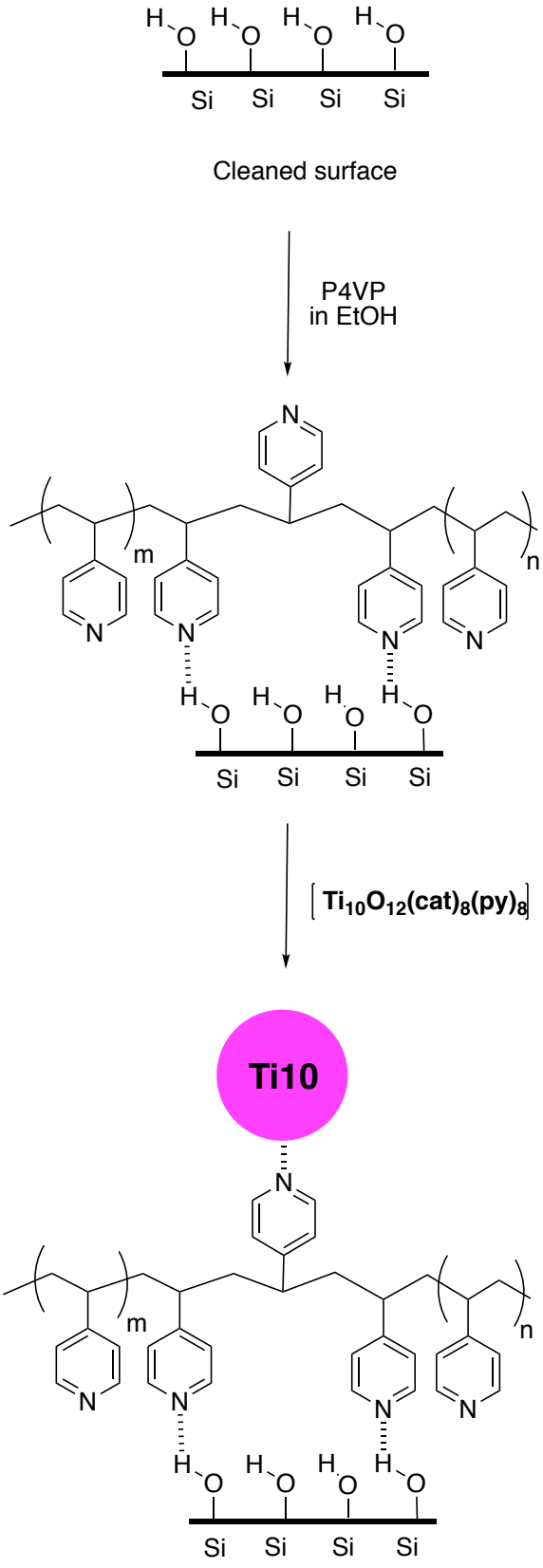

Figure 8: A schematic representation of the procedure for the two steps functionalization of a surface by a hybrid thin film based on the $[Ti_{10}O_{12}(cat)_8(py)_8]$ cluster. A first step consists in the formation of a P4VP thin film interacting with the surface through hydrogen bonds. In the next step, the $[Ti_{10}O_{12}(cat)_8(py)_8]$ complex is coordinated to the P4VP anchored onto the surface. It should be mentioned that the accurate number of P4VP pyridines linked to the cluster could not be determined. Multilayers are generated starting from the surface functionalized with the hybrid film, after multiple treatments with the P4VP solution followed by the cluster solution.

In a first attempt, a quartz surface (microscope slide) treated beforehand with a Piranha solution is dipped into an ethanol P4VP solution (1% w/w). The UV-visible transmission spectrum of the functionalized quartz slides displays a band centred at λ = 260 nm attributed to the $\pi \rightarrow \pi^*$ transitions of the P4VP pyridines. The resulting quartz surface is then treated with a second solution containing the $[Ti_{10}O_{12}(cat)_8(py)_8]$ complex. Although no clear modification of the surface appearance is noticed to the naked eye, a large continuous weak band in the visible region below λ = 550 nm is detected by UV-visible spectroscopy. It is noteworthy that the same result is obtained when the cleaned glass surface is directly immersed in the $[Ti_{10}O_{12}(cat)_8(py)_8]$ solution without a pretreatment with P4VP.

Next, the thickness of these films is evaluated by ellipsometry. As this technique requires reflective surfaces, the films were prepared on silicon wafers with a native SiO_2 layer which were cleaned with a Piranha solution. The surface chemistry of the substrate is thus similar for silicon wafers as for quartz or glass slides, and one can assume that the thin film structure and thickness is identical on those substrates. As the complex refractive index of the hybrid material is not known, we impose a constant refractive index in the fitting procedure of the ellipsometry data, which leads to thickness values that are slightly different from the real ones, but which are close enough to monitor with a good precision the growth of the thin films on the substrate.[29] The measured values are compiled in table 1. The values given are an average of the thickness measured on >10 points on the surface, and the standard deviation

(which is much higher than the instrumental standard deviation) thus represents the homogeneity of the thin film.

The wafer is first immersed in a P4VP ethanol solution with a concentration of 0.01 % w/w, 0.1 % w/w or 1% w/w. The homogeneity of the films is correlated with the P4VP solution concentration. For the two highest concentrations (*i.e.* 0.1 % w/w and 1% w/w), the thickness of the films are respectively found to be 0.8 ± 0.2 nm and 0.9 ± 0.2 nm (see Table 1). The measurements performed at different spots on the wafers show no significant variation of the film thickness, therefore we conclude that the thin films cover homogeneously the silicon wafer surfaces. At the 0.01 % w/w concentration, the results are not reproducible and important thickness differences are determined by varying the spots of measurement on the wafer. These wafers homogeneously covered by the P4VP polymer are next dipped in a CH_2Cl_2 solution of $[Ti_{10}O_{12}(cat)_8(py)_8]$ ($c = 5.10^{-4}$ $mol.L^{-1}$). The thickness of the hybrid films reaches only a few nanometers. As mentioned just before, we highlighted that $[Ti_{10}O_{12}(cat)_8(py)_8]$ could be directly grafted on a glass surface without the presence of the P4VP film. However, the ellipsometry study clearly indicates an inhomogeneous deposition of the cluster with thickness ranging from 25.3 to 81.6 nm. This indicates undoubtedly the presence on the surface of aggregates rather than a homogeneous sediment. Also, this proves the indispensable functionalisation of SiO_2 surfaces by P4VP beforehand to generate homogeneous films incorporating the cluster.

Film	Thickness (nm)
P4VP-1%	0.9 ± 0.2
P4VP-0.1%	0.8 ± 0.2
P4VP-1% -Ti_{10}	3.2 ± 0.3
P4VP-0.1% -Ti_{10}	4.0 ± 1
LbLx2	9.2 ± 1.0
LbLx3	16.1 ±1.9

Table 1: Thickness of the hybrid films evaluated by ellipsometry.

Furthermore, the process can be repeated several times in order to build alternated layers of polymer and cluster on the surface by using a layer-by-layer approach.[30] Clearly, we observe that the thickness of the film increase with the number of layers adsorbed.

Overall, our approach allows us to generate LbL hybrid films and to control the amount of oxo-cluster deposited on the surface. Also, the thickness of the films can be tuned by varying the number of layers.

Conclusion

We have reported an oxo-cluster-based hybrid material absorbing light in the visible domain. The straightforward synthesis permitting to access to this material requires only very accessible starting materials such as $[Ti_{10}O_{12}(cat)_8(py)_8]$ and poly(4-vinylpyridine) and does not require particular care. The strategy allowing the formation of the hybrid material is unique for titanium oxo-cluster-based hybrid material, as it takes advantage of the labile behaviour of the pyridine ligands decorating the inorganic core of the complex. Importantly, the incorporation of the oxo-cluster $[Ti_{10}O_{12}(cat)_8(py)_8]$ in the organic polymeric matrix is quantitative and does not lead to any degradation or significant modification of the oxo-cluster backbone. Furthermore, the resulting solid is homogenous as proven by Raman spectroscopy and ^{13}C CP MAS NMR investigations.

Finally, we have shown that SiO_2 surfaces can be functionalized following a Layer-by-Layer approach by alternate depositions of P4VP and of the titanium oxo-cluster. The thickness of the thin film can thus be finely tuned by varying the number of deposition steps, down to 4 nm for a monolayer. Current investigations are devoted to characterize the physical properties of these films and hybrid materials. In particular, efforts are focused on the study of the interactions of these materials with light.

Acknowledgments

We warmly thank Dr. J. Raya for solid-state cross-polarization magic angle spinning (CP/MAS) ^{13}C NMR spectra measurement. Also, we thank the Centre National de la Recherche Scientifique (CNRS) and the University of Strasbourg (UDS) for financial support.

Experimental part

All reagents and products were purchased from Sigma Aldrich, Alfa Aesar or TCI and used as received. Solid-state cross-polarization magic angle spinning (CP/MAS) ^{13}C NMR spectra were recorded on a Bruker Avance 500 spectrometer at ambient temperature with a magic angle spinning rate of 12.0 kHz. All Raman spectra were recorded with an InVia Renishaw spectrum equipped with a CCD (charge coupled device) as a detector. All experiments were carried at a resolution of 1 cm^{-1} with an exposure time of 10 s and an excitation wavelength of 514 nm provided by an Argon STELLAR laser. Infrared (IR) spectra were recorded with a

Perkin-Elmer FT-IR spectrometer. Solid-state measurements were performed on a Perkin-Elmer LS 55 spectrometer. Thermogravimetric analyses (TGA) were performed on a Perkin-Elmer Pyris 6 TGA analyzer.

For the thickness measurements a spectroscopic ellipsometer was used (SE800, SENTECH). The film was modeled as a single layer with a constant complex refractive index $n = n_0 + i\, n_1$, with n_0=1.465 and n_1=36. The thickness of the cleaned SiO_2 substrate was fixed at 2.4 nm.

Synthesis of P4VPTiXX% hybrid material

To a stirred solution of P4VP (60 mg) in $CHCl_3$ (5 mL) was added dropwise under agitation the appropriate amount of $[Ti_{10}O_{12}(cat)_8(py)_8]$ dissolved in $CHCl_3$ (3 mL). The precipitate was filtered, washed several times with $CHCl_3$ and then dried under vacuum during one night before analysis. When no precipitate was formed, the solvent was removed by evaporation under vacuum and the residue was dried before analysis.

Functionalization and grafting of the $[Ti_{10}O_{12}(cat)_8(py)_8]$ complex on a silicon wafer

The functionalization of the different substrates was performed by dip-coating. Prior to functionalization, the substrate was cleaned with a Piranha solution for 15 min, rinsed with distilled water and dried under argon.

Poly(4-vinylpyridine) deposition: the clean substrate was immersed in a solution of P4VP (0.01%, 0.1% or 1%) in ethanol. After 2 h, the substrate was washed several times with ethanol and dried under argon.

$[Ti_{10}O_{12}(cat)_8(py)_8]$ grafting: the titanium complex was grafted on the previously functionalized P4VP surfaces by placing the substrate in a 5.10^{-4} M solution of $[Ti_{10}O_{12}(cat)_8(py)_8]$ in chloroform. After 2 hours, the surface was rinsed several times with chloroform and dried under argon.

Multilayers were generated from a silicon wafer firstly dipped in a P4VP solution in ethanol (1 %) and next immersed in a 5.10^{-4} M solution of $[Ti_{10}O_{12}(cat)_8(py)_8]$ in dichloromethane. After 2 hours, the surface was rinsed with ethanol and dried under argon. Next, this functionalized wafer is immersed in a P4VP solution in dichloromethane (1 %) followed by a treatment with the $[Ti_{10}O_{12}(cat)_8(py)_8]$ solution.

[1] G. Kickelbick, Hybrid Materials: Synthesis, Characterization, and Applications, Wiley-VCH Verlag GmbH & Co. KGaA (2007). For articles about hybrid materials see: M. Amela-Cortes, Y. Molard, S. Paofai, A. Desert, J.-L. Duvail, N. G. Naumovd and S. Cordier, *Dalton Trans.*, 2016, **45**, 237–245 ; A. Garreau, F. Massuyeau, S. Cordier, Y. Molard, E. Gautron, P.

Bertoncini, E. Faulques, J. Wery, B. Humbert, A. Bulou, and J.-L. Duvail, *ACS Nano*, 2013, *7*, 2977–2987 ; X. Luo, J. Han, Y. Ning, Z. Lin, H. Zhang and B. Yang, *J. Mater. Chem.*, 2011, **21**, 6569–6575; S. Li, M. S. Toprak, Y. S. Jo, J. Dobson, D. K. Kim and M. Muhammed, *Adv. Mater.*, 2007, **19**, 4347–4352; S. Gross, G. Trimmel, U. Schubert and V. D. Noto, *Polym. Adv. Technol.*, 2002, **13**, 254–259.

[2] F. Wang, S. Min, Y. Han and L. Feng, *Superlattices Microstruct.*, 2010, **48**, 170-180.
[3] Muder AL Haydar, Hussein Rasool Abid, Bruce Sunderland and Shaobin Wang, *Drug Des Devel Ther*. 2017, **11**, 2685–2695; R. Liu, T. Yu, Z. Shi and Z. Wang, *Int J Nanomedicine*. 2016, **11**, 1187–1200.
[4] P. J. Rivero, J. A. Garcia, I. Quintana and R. Rodriguez *Coatings*, 2018, *8*, 76; doi:10.3390/coatings8020076.
[5] B. Lebeaua and P. Innocenzi *Chem. Soc. Rev.*, 2011, **40**, 886-906.
[6] W.-H. Fang, L. Zhang and J. Zhang *Chem. Soc. Rev.,* 2018, **47**, 404-421; L. Rozes and C. Sanchez *Chem. Soc. Rev.*, 2011, **40**, 1006–1030.
[7] L. Rozes, N. Steunou, G. Fornasieri, and C. Sanchez *Monatshefte für Chemie*, 2006, 137, 501–528.
[8] C. Sanchez, GJ de AA Soler-Illia, F. Ribot and D. Grosso, CR Chimie, 2003, 1131; GJ de AA Soler-Illia, C. Sanchez, B. Lebeau and J. Patarin, *Chem Rev*, 2002, **102**, 4093; CG Goltner and M. Antonietti, *Adv. Mater.*, 1997, **9**, 431.
[9] G. Fornasieri, L. Rozes, S. Le Calvé, B. Alonso, D. Massiot, M. N. Rager, M. Evain,| K. Boubekeur, and C. Sanchez *J. Am. Chem. Soc.*, 2005, **127**, 4869-4878.
[10] C. Chaumont, P. Mobian and M. Henry *Dalton Trans.*, 2014, **43**, 3416–3419.
[11] C. Chaumont, A. Chaumont, N. Kyritsakas, P. Mobian and M. Henry *Dalton Trans.*, 2016, **45**, 8760-8769.
[12] C. Chaumont, E. Huen, C. Huguenard, P. Mobian and M. Henry, *Polyhedron*, 2013, **57**, 70−76; K. Gigant, A. Rammal, M. Henry, *J. Am. Chem. Soc.*, 2001, **123**, 11632−11637; P. Persson, R. Bergstrom and S. Lunell, *J. Phys. Chem. B*, 2000, **104**, 10348−10351.
[13] H. Assi, G. Mouchaham, N. Steunou, T. Devic and C. Serre, *Chem. Soc. Rev.,* 2017, **46**, 3431-3452.
[14] L. M. Robinson and D. F. Shriver, *J. Coord. Chem.*, 1996, **37**, 119-129 ; J. A. Jackson, M. D. Newsham, C. Worsham, and D. G. Nocera, *Chem. Mater.*, 1996, **8**, 558–564.
[15] J. Pardey, A. D. Rojas, J. E. Yánez, P. Betancourt, C. Scott, C. Chinea, C. Urbina, D. Moronta and C. Longo, *Polyhedro*n, 2005, **24**, 511; J. Albadi, M. Keshavarz, F. Shirini and M. Vafaie-nezhad, *Catal. Commun.*, 2012, **27**, 17; J. Albadi, F. Shirini, J. Abasi, N. Armand and T. Motaharizadeh, *C. R. Chimie*, 2013, **16**, 407 ; G. Jeschke, *J. Phys. Chem. B*, 2000, **104**, 8382.
[16] U. Caruso, R. Centore, B. Panunzi, A. Roviello and A. Tuzi, *Eur. J. Inorg. Chem.*, 2005, 2747.
[17] D. H. Lee, S. H. Han, W. Joo and J. K. Kim, *Macromolecules*, 2008, **41**, 2577.

[18] M. P. McCurdie and L. A. Belfiore, *Polymer*, 1999, **40**, 2889 ; T. Shimidzu, K. Izaki, Y. Akai and T. Iyoda, *Polymer Journal*, 1981, **13**, 889 ; J. M. Calvert and T. J. Meyer, *Inorg. Chem.*, 1982, **21**, 3978.
[19] A. Rahmatpour, N. Goodarzi, *Catal. Comm.* doi.org/10.1016/j.catcom.2018.11.001 ; A.L. Santana, L.K. Noda, A.T.N. Pires, J.R. Bertolino, *Polymer Testing*, 2004, **23**, 839–845.

[20] L. A. Belfiore, A. T. N. Pires, Y. Wang, H. R. J. Graham and E. Ueda, *Macromolecules*, 1992, **25**, 1411; L. A. Belfiore, H. R. J. Graham, E. Ueda and Y. Wang, *Polym. Int.*, 1992, **28**, 81.
[21] O. P. Pandey, S. K. Sengupta, M. K. Mishra and C. M. Tripathi, *Bioionorg. Chem. Appl.*, 2003, **1**, 35.
[22] R. L. Garrell and K. D. Beer, Langmuir, 1989, **5**, 452–458.
[23] S. J. Greaves and W. P. Griffith *Spectrochimica Acta*, 1991, **47A**, 133-140.
[24] H. Senouci, B. Millet, C. Volkringer, C. Huguenard, F. Taulelle and M. Henry *C. R. Chimie*, 2010, **13**, 69-96.
[25] The very minor signals at 25 ppm in Figure 5c and 5a are impurities arising from P4VP.
[26] P. Kubelka and F. Munk *Z. tech. Phys.*, 1931, **12**, 593-601.
[27] G. Khalil, C. Orvain, L. Fang, L. Barloy, A. Chaumont, C. Gaiddon, M. Henry, N. Kyritsakas and P. Mobian *Dalton Trans.*, 2016, **45**, 19072-19085.
[28] J. Raczkowska, Y. Stetsyshyn, K. Awsiuk, J. Zemła, A. Kostruba, K. Harhay, M. Marzec, A. Bernasik, O. Lishchynskyi, H. Oharb and A. Budkowskia, *RSC Adv.*, 2016, **6**, 87469-87477; S. Malynych, I. Luzinov, G. Chumanov, *J. Phys. Chem. B* 2002, **106**, 1280–1285 ; J. M. Clear, J. M. Kelly, J. G. Vos, *Die Makromol. Chemie* 1983, **184**, 613–625.
[29] R. Merindol, S. Diabang, O. Felix, T. Roland, C. Gauthier and G. Decher, *ACS Nano*, 2015, **9**, 1127-1136.
[30] J. J. Richardson, J. Cui, M. Björnmalm, J. A. Braunger, H. Ejima and F. Caruso, *Chem. Rev.* 2016, **116**, 14828−14867.